A robust thermal-energy-storage property associated with electronic phase transitions for quadruple perovskite oxides

COMMUNICATION

Robust thermal-energy-storage property associated with electronic phase transitions for quadruple perovskite oxides

Tasuku Uchimura,[a] Ikuya Yamada,[a,*]

Received 00th January 20xx,
Accepted 00th January 20xx

DOI: 10.1039/x0xx00000x

The quadruple perovskite oxides RCu$_3$Fe$_4$O$_{12}$ (R: rare-earth metals) exhibit large latent-heat capacities (25 J g^{-1} at maximum) with variable transition temperatures between 254 and 365 K, whereas their transition entropies are almost retained. This finding proposes an effective way to design robust thermal-energy-storage materials with various operating temperatures.

The efficient utilization of unused energy, such as exhaust heat from factories and vehicles, is a fundamental issue to achieve sustainable development. Thermal-energy-storage (TES) materials, which can charge/discharge unused energy, have been extensively studied because of the simple and useful feature.[1–3] Several types of TES materials applying sensible heat, chemical reaction heat, and latent heat are suggested. Typical latent-heat TES materials are based on liquid-solid phase transitions because of high TES capacity such as water (334 J g^{-1} at 273 K), and erythritol (340 J g^{-1} at 391 K). However, it is challenging to control transition temperature for wide-ranging temperatures of exhaust heat emitted from various industries because of the stiffness of transition temperatures for liquid-solid phase transitions.

Solid-solid phase transitions for transition metal oxides have been investigated as alternative TES materials with variable operating temperatures.[4,5] Vanadium dioxide (VO_2) is known as a typical TES material with a large latent heat capacity of about 50 J g^{-1} at 340 K,[6] whose origin is explained by the simultaneous change in the degree of freedom of charge (metal-insulator transition, MIT), spin (antiferromagnetic transition), and orbital (orbital ordering). The transition temperature can be controlled by chemical substitution of transition metals (W and Cr) for V [i.e., V_{1-x}(Cr, W)$_x$O$_2$], leading to significantly wide operating temperature ranges between 206 and 480 K.[7,8] However, the latent-heat capacity substantially decreases down to 15 J g^{-1} with doping. This arouses interest in novel TES materials with controllable operating temperatures and robust latent-heat capacities.

We focus on the RCu$_3$Fe$_4$O$_{12}$ family (R: rare-earth metals) and its remarkable electronic phase transitions. This series is synthesized under high pressure up to 15 GPa, and crystallizes in the quadruple perovskite structure, in which two different transition metals of Cu and Fe occupy the distinct crystallographic sites of pseudosquare A'- and octahedral B-sites, respectively (Figure 1).[9] This oxide undergoes two different types of electronic phase transitions, depending on the ionic size of R ion: intersite charge-transfer (ICT: $3Cu^{2+} + 4Fe^{3.75+} \rightleftarrows 3Cu^{3+} + 4Fe^{3+}$ for R = La, Pr, Nd, Sm, Eu, Gd, Tb) and charge-disproportionation transitions (CD: $8Fe^{3.75+} \rightleftarrows 5Fe^{3+} + 3Fe^{5+}$ for R = Dy, Ho, Er, Tm, Yb, Lu, Y),[10–12] in which metal-insulator (ICT)/metal-semiconductor (CD) and antiferromagnetic (ICT)/ferrimagnetic (CD) transitions simultaneously occur. The coincident change in the degree of freedom of charge, spin, and probably orbital may induce large latent heat. Together with the fact that the phase transition temperatures for ICT can be controlled between 360 (R = La) and 230 K (R =Tb) by substituting R ions, promising performance as latent-heat TES materials is expected. However, since detailed thermal analysis has not been conducted, the potential as latent-heat TES materials is unclear. In this study, we investigate calorimetric properties for RCu$_3$Fe$_4$O$_{12}$ (R = La, Pr, Nd, Sm, Gd, Dy). The differential scanning calorimetry (DSC) analysis indicates that large latent-heat capacities up to 25 J g^{-1} are involved in the ICT transitions with various transition temperatures between 253 and 368 K. The transition entropies are retained at about 0.06 J g^{-1} K^{-1}, which are independent on the transition temperatures, unlike the significant reduction in transition entropies with Cr, W-doping for V_{1-x}(Cr, W)$_x$O$_2$. These findings propose that RCu$_3$Fe$_4$O$_{12}$ are the promising latent-heat TES materials with wide-ranging operating temperatures and essential performance.

The polycrystalline samples of RCu$_3$Fe$_4$O$_{12}$ (R =La, Pr, Nd, Sm, Gd, Dy) were synthesized by using a high-pressure method according to the literature (see ESI for details).[11] X-ray powder

[a] Department of Materials Science, Graduate School of Engineering, Osaka Prefecture University, 1-2 Gakuen-cho, Naka-ku, Sakai, Osaka 599-8570, Japan E-mail: yamada@mtr.osakafu-u.ac.jp

†Electronic Supplementary Information (ESI) available: Experimental details. material characterization. See DOI: 10.1039/x0xx00000x

diffraction (XRD) measurement was performed using a powder X-ray diffractometer with Cu-Kα radiation (Ultima IV, Rigaku, Japan). Synchrotron X-ray diffraction (SXRD) data were collected at temperatures between 200 and 400 K for $LaCu_3Fe_4O_{12}$ and $GdCu_3Fe_4O_{12}$ with a Debye-Scherrer camera installed at the BL02B2 beamline of SPring-8, Japan.[13] Crystal structure refinement was conducted based on the SXRD data using the Rietveld refinement program RIETAN-FP.[14] DSC data were obtained at temperatures between 125 and 500 K using Hitachi DSC7020. Heating and cooling rates were 10 ºC min^{-1}, and N_2 gas was used as protective and purging gas. Latent-heat capacity was estimated from the integrated areas of endo/exothermic peaks.

Figure 2 shows the XRD patterns for $RCu_3Fe_4O_{12}$. The primary phases for all were indexed with the cubic quadruple perovskite structure with 1:3 ordering of *R* and Cu ions at *A*-sites. Although small amount (4–7 wt%) of impurities, α-Fe_2O_3 and CuO, were observed for *R* = Pr and Nd, we considered that these phases do not significantly affect the thermodynamic properties because no phase transitions are expected in the temperature range of interest in this study.[15,16]

Figure 3 displays the DSC curves on heating and cooling processes for $RCu_3Fe_4O_{12}$. Significant endothermic/exothermic peaks were observed for *R* = La, Pr, Nd, Sm, Gd at ICT transition temperatures, as expected from the previous report.[11] These observations indicate the first-order feature with large latent-heat capacities for ICT transitions. The latent-heat capacities, i.e., transition enthalpies (ΔH), were calculated from the average of the endothermic and exothermic peak areas (see the detailed data in Table S1 in ESI). The calculated specific latent-heat capacity for $LaCu_3Fe_4O_{12}$ was about 25 J g^{-1}, corresponding to the volume latent-heat capacity of 154 J cm^{-3}. This value is much larger than those for perovskite-related oxides, $YBaFe_2O_5$ (37.2 J cm^{-3})[17] and $BaTiO_3$ (5.42 J cm^{-3}),[18] approaching that for VO_2 (234 J cm^{-3}).[6] The observed latent heat for $LaCu_3Fe_4O_{12}$ indicates that the ICT transitions are associated with the change in the degree of freedom of charge (MIT), spins, and probably orbitals, the latter of which corresponds to the change in entropy of $k_B \ln 2$, because the orbital degeneracy of e_g orbitals for Fe^{4+} ions in octahedral coordination ($t_{2g}^3e_g^1$ configuration) is removed for Fe^{3+} ions ($t_{2g}^3e_g^2$ configuration) by ICT transition. This feature is retained for *R* = Pr, Nd, Sm, and Gd, in which the ICT temperatures decrease with shrinkage of *R* ions, as reported previously,[11] although broadening and weakening of endothermic/exothermic peaks were observed for oxides with smaller *R* ions, as discussed later. In contrast, the endothermic/exothermic peaks were much smaller (4.42 J g^{-1}) at the CD transition for $DyCu_3Fe_4O_{12}$, indicating the second-order character of CD transition.

The broadening of peaks for the DSC curves of $GdCu_3Fe_4O_{12}$ was investigated by using temperature-variable SXRD. Figure 4 demonstrates the fraction of the high-temperature phase for $LaCu_3Fe_4O_{12}$ and $GdCu_3Fe_4O_{12}$ estimated by Rietveld refinement of the SXRD data (Figure S1 and Table S2 in ESI). The coexistence of the HT and LT phases was observed only at 380 K for $LaCu_3Fe_4O_{12}$, whereas predominant on a broader temperature range between 210 and 270 K for $GdCu_3Fe_4O_{12}$. The difference in the two-phase-coexistence temperature is consistent with the DSC data. This is probably because the compounds with lower ICT transition temperatures may tend to undergo the overheating and overcooling.

Figure 5a shows the specific transition enthalpy (ΔH) as a function of transition temperature for $RCu_3Fe_4O_{12}$ (*R* = La, Pr, Nd, Sm, Gd). $RCu_3Fe_4O_{12}$ series covers a wide temperature range between 253 and 368 K, as well as $V_{1-x}W_xO_2$. The latent-heat capacity for $RCu_3Fe_4O_{12}$ gradually decreases from 25 J g^{-1} (*R* = La) to 15 J g^{-1} (*R* = Gd) when the transition temperature is lowered by smaller *R* ions, implying the degradation of TES performance by elemental substitution like $V_{1-x}W_xO_2$ at first glance.[7] The estimated reduction rate of ΔH was about 30% and 50% per 100 K for $RCu_3Fe_4O_{12}$ and $V_{1-x}W_xO_2$, respectively. To conduct a detailed thermodynamic analysis, we calculated the specific transition entropies (ΔS) based on the thermodynamic relation of $\Delta S = \Delta H/T_t$, where T_t is the transition temperature. Figure 5b displays ΔS as a function of transition temperature for $RCu_3Fe_4O_{12}$. The ΔS values for $RCu_3Fe_4O_{12}$ are almost constant at 0.06 J g^{-1} K^{-1}. A linear fitting estimates the reduction rate to be only 8% per 100 K. On the other hand, ΔS for $V_{1-x}W_xO_2$ drastically decreased from 0.15 J g^{-1} K^{-1} (*x* = 0) to 0.07 J g^{-1} K^{-1} (*x* = 0.05), corresponding to the reduction rate of 40% per 100 K. Consequently, ΔS, which is considered to be the essential TES property independent on T_t, is retained at almost constant by *R*-substitution for $RCu_3Fe_4O_{12}$. The apparent decrease in ΔH for $RCu_3Fe_4O_{12}$ is primarily attributed to the lowering in T_t, as supported by the spectroscopic study that the electronic states and transformations for $RCu_3Fe_4O_{12}$ are essentially unchanged by *R*-substitution.[11] In contrast, ΔS is decreased by doping for $V_{1-x}(W, Cr)_xO_2$, which substantially alters the electronic states from VO_2 because of difference in the valences (e.g., W^{6+} instead of V^{4+}) and electron configurations (e.g., t_{2g}^2 for Cr^{4+} and t_{2g}^1 for V^{4+}) disturbing the intrinsic electronic state for VO_2.[19–21] These results lead us to a simple conclusion that the substitution of atoms indirectly related to electronic states (*R* ions for $RCu_3Fe_4O_{12}$), not the crucial atoms to form the electronic states (Cu and Fe ions for $RCu_3Fe_4O_{12}$), can keep essential TES properties and adjust the transition temperatures.

The above conclusion is supported by the comparison with $LaCu_3Fe_{4-x}Mn_xO_{12}$. According to the literature,[22] the increase in Mn content for $LaCu_3Fe_{4-x}Mn_xO_{12}$ (*x* = 0, 0.1, 0.5, 0.75, 1) gradually decreases the transition temperature from 365 to 292 K, together with the significant relaxation of the phase transition leading to the second-order character. The ΔH value decreases from 25 (*x* = 0) to 1.5 J g^{-1} (*x* = 1) and ΔS from 0.06 (*x* = 0) to 0.007 J g^{-1} K^{-1} (*x* = 0). Since this is more similar to the intrinsic reduction in ΔS for $V_{1-x}W_xO_2$ rather than almost constant ΔS for $RCu_3Fe_4O_{12}$, we can conclude that the substitution of the crucial element (Fe) degrades the TES performance.

In summary, we describe that the substitution of *R* ion for $RCu_3Fe_4O_{12}$ achieves the control of operating temperature for latent-heat TES material with maintaining the intrinsic transition entropy, that is, essential latent-heat property. This finding suggests that the substitution of the atoms indirectly related to electronic state can keep essential TES property and control transition temperature.

The authors thank Satoshi Tsutsui for fruitful discussion. The synchrotron radiation experiments were performed at SPring-8 under the approval of the Japan Synchrotron Radiation Institute (proposal number 2019A1476 and 2019B1420). This work was supported by JSPS KAKENHI (grant number JP18H03835, JP19H02438, and JP20H02825).

Conflicts of interest

There are no conflicts to declare.

References

1 L. Miró, J. Gasia and L. F. Cabeza, Thermal energy storage (TES) for industrial waste heat (IWH) recovery: A review. *Appl. Energy*, 2016, **179**, 284–301.
2 I. Sarbu and C. Sebarchievici, A comprehensive review of thermal energy storage. *Sustainability* 2018, **10**, 191.
3 S. M. Hasnain, Review on sustainable thermal energy storage technologies, part II: Cool thermal storage. *Energy Convers. Manag.*, 1998, **39**, 1139–1153.
4 F. J. Morin, Oxides which show a metal-to-insulator transition at the neel temperature. *Phys. Rev. Lett.*, 1959, **3**, 34–36.
5 J. B. Goodenough, The two components of the crystallographic transition in VO_2. *J. Solid State Chem.*, 1971, **3**, 490–500.
6 G. V Chandrashekhar, H. L. C. Barros and J. M. Honig, Heat capacity of VO_2 single crystals. *Mater. Res. Bull.*, 1973, **8**, 369–374.
7 S. Niitaka, H. Takagi, M, Miyano, *Jpn. Pat.*, JP2010163510A, 2010.
8 S. Niitaka, H. Takagi, K. Kono, *Euro. Pat.*, EP2987841, 2016.
9 K. Momma and F. Izumi, VESTA 3 for three-dimensional visualization of crystal, volumetric and morphology data. *J. Appl. Crystallogr.*, 2011, **44**, 1272–1276.
10 Y. W. Long, N. Hayashi, T. Saito, M. Azuma, S. Muranaka and Y. Shimakawa, Temperature-induced A-B intersite charge transfer in an A-site-ordered $LaCu_3Fe_4O_{12}$ perovskite. *Nature*, 2009, **458**, 60–63.
11 I. Yamada, H. Etani, K. Tsuchida, S. Marukawa, N. Hayashi, T. Kawakami, M. Mizumaki, K. Ohgushi, Y. Kusano, J. Kim, N. Tsuji, R. Takahashi, N. Nishiyama, T. Inoue, T. Irifune and M. Takano, Control of bond-strain-induced electronic phase transitions in iron perovskites. *Inorg. Chem.*, 2013, **52**, 13751–13761.
12 H. Etani, I. Yamada, K. Ohgushi, N. Hayashi, Y. Kusano, M. Mizumaki, J. Kim, N. Tsuji, R. Takahashi, N. Nishiyama, T. Inoue, T. Irifune and M. Takano, Suppression of intersite charge transfer in charge-disproportionated perovskite $YCu_3Fe_4O_{12}$. *J. Am. Chem. Soc.*, 2013, **135**, 6100–6106.
13 S. Kawaguchi, M. Takemoto, K. Osaka, E. Nishibori, C. Moriyoshi, Y. Kubota, Y. Kuroiwa and K. Sugimoto, High-throughput powder diffraction measurement system consisting of multiple MYTHEN detectors at beamline BL02B2 of SPring-8. *Rev. Sci. Instrum.*, 2017, **88**, 85111.
14 F. Izumi and K. Momma, Three-Dimensional Visualization in Powder Diffraction. *Solid State Phenom.*, 2007, **130**, 15–20.
15 A. C. Vajpei, F. Mathieu, A. Rousset, F. Chassagneux and J. M. Letoffe, Differential scanning calorimetry studies on influence of microstructure on transformation. *J. Therm. Anal.*, 1987, **32**, 857–863.
16 X. G. Zheng, T. Kawae, S. Tanaka, M. Suzuki and C. N. Xu, Single-crystalline CuO by DSC heat capacity measurement. *J. Therm. Anal. Calorim.*, 1999, **57**, 853–858.
17 P. Karen, Chemistry and thermodynamics of the twin charge-ordering transitions in $R BaFe_2O_{5+w}$ series. *J. Solid State Chem.*, 2004, **177**, 281–292.
18 P. K. Dutta, R. Asiaie, S. A. Akbar and W. Zhu, Hydrothermal Synthesis and Dielectric Properties of Tetragonal $BaTiO_3$. *Chem. Mater.*, 1994, **6**, 1542–1548.
19 C. Tang, P. Georgopoulos, M. E. Fine, J. B. Cohen, M. Nygren, G. S. Knapp and A. Aldred, Local atomic and electronic arrangements in $W_xV_{1-x}O_2$. *Phys. Rev. B*, 1985, **31**, 1000–1011.
20 X. Tan, T. Yao, R. Long, Z. Sun, Y. Feng, H. Cheng, X. Yuan, W. Zhang, Q. Liu, C. Wu, Y. Xie and S. Wei, Unraveling metal-insulator transition mechanism of VO_2 triggered by tungsten doping. *Sci. Rep.*, 2012, **2**, 466.
21 Y. Wu, L. Fan, W. Huang, S. Chen, S. Chen, F. Chen, C. Zou and Z. Wu, Depressed transition temperature of $W_xV_{1-x}O_2$: Mechanistic insights from the X-ray absorption fine structure (XAFS) spectroscopy. *Phys. Chem. Chem. Phys.*, 2014, **16**, 17705–17714.
22 I. Yamada, S. Marukawa, M. Murakami and S. Mori, "True" negative thermal expansion in Mn-doped $LaCu_3Fe_4O_{12}$ perovskite oxides. *Appl. Phys. Lett.*, 2014, **105**, 231906.

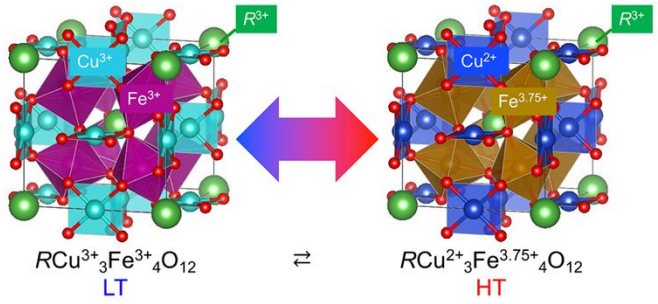

Figure 1. Schematics of crystal structure and intersite charge-transfer phase transition for $RCu_3Fe_4O_{12}$. The valence states for low-temperature (LT) and high-temperature (HT) phases are represented. The crystal structures were drawn by using the VESTA-3 software.[9]

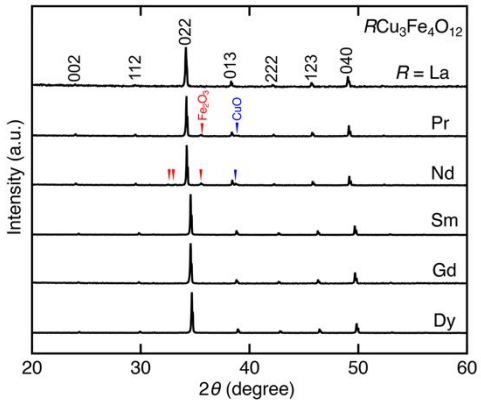

Figure 2. XRD patterns for $RCu_3Fe_4O_{12}$. Selected *hkl* reflections are indexed.

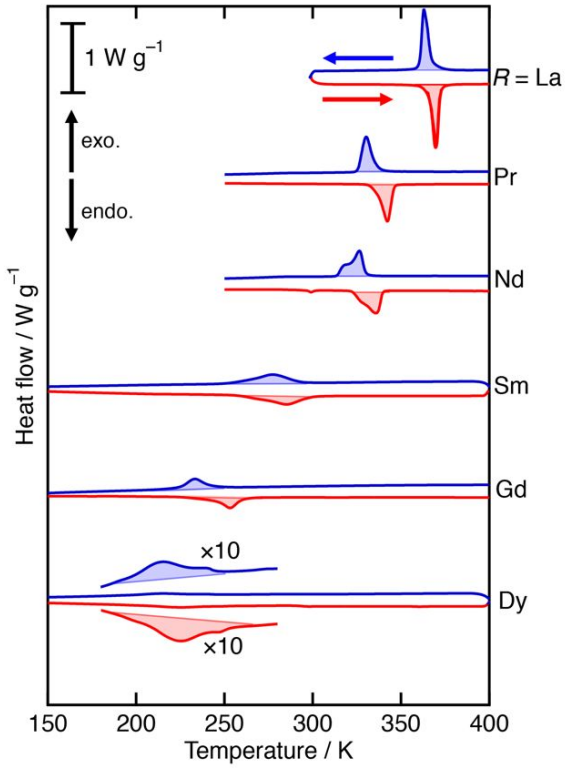

Figure 3. DSC curves in heating (red) and cooling (blue) processes for $RCu_3Fe_4O_{12}$ (R = La, Pr, Nd, Sm, Gd, and Dy). Each profile is separated by an offset of 1.5 W g^{-1}. The tenfold enlarged profiles are also represented for $DyCu_3Fe_4O_{12}$.

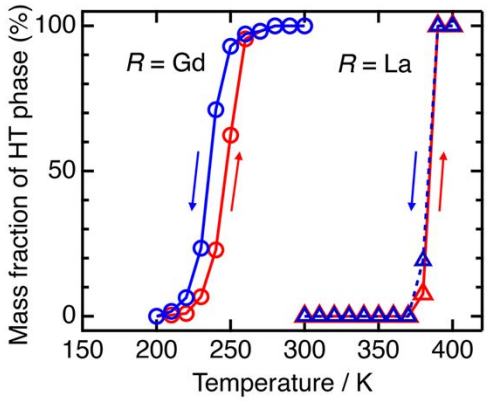

Figure 4. Mass fractions of high-temperature (HT) phase for $LaCu_3Fe_4O_{12}$ and $GdCu_3Fe_4O_{12}$ on heating (red) and cooling (blue) processes obtained from the Rietveld analysis of synchrotron X-ray diffraction data.

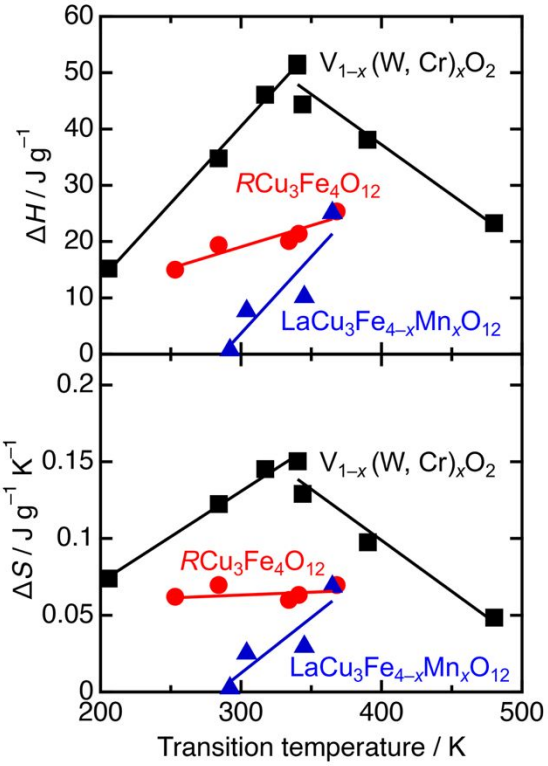

Figure 5. (a) Specific transition enthalpy (ΔH) and (b) specific transition entropy (ΔS) as a function of transition temperature for $RCu_3Fe_4O_{12}$ (R = La, Pr, Nd, Sm, Gd) red circles), $V_{1-x}(W, Cr)_xO_2$ (black squares), and $LaCu_3Fe_{4-x}Mn_xO_{12}$ (blue triangles). The data for $V_{1-x}(W, Cr)_xO_2$ and $LaCu_3Fe_{4-x}Mn_xO_{12}$ were taken from the references.[7,8,22]